Additive Manufacturing 35 (2020) 101298

Contents lists available at ScienceDirect

Additive Manufacturing

journal homepage: www.elsevier.com/locate/addma

Unique coding for authentication and anti-counterfeiting by controlled and random process variation in L-PBF and L-DED

Daniel Eisenbarth[a,*], Philipp Stoll[a], Christoph Klahn[a], Timon B. Heinis[b], Mirko Meboldt[b], Konrad Wegener[c]

[a] inspire AG, ETH Zürich, Technoparkstrasse 1, 8005 Zürich, Switzerland
[b] Product Development Group Zurich, ETH Zürich, Leonhardstrasse 21, 8092 Zürich, Switzerland
[c] Institute of Machine Tools and Manufacturing, ETH Zürich, Leonhardstrasse 21, 8092 Zürich, Switzerland

ARTICLE INFO

Keywords:
Powder bed fusion
Directed energy deposition
Coding
Anti-counterfeiting
Eddy current testing

ABSTRACT

Additive manufacturing technologies enable various possibilities to create and modify the material composition and structure on a local level, but are often prone to undesired defects and inhomogeneities. This contribution makes use of such flaws to generate material-inherent, hidden codes and watermarks in metals for authentication and anti-counterfeiting applications. By controlled and random process variation, unique codes that can be read and authenticated by an eddy current device were produced with the processes of laser powder bed fusion (L-PBF) and laser directed energy deposition (L-DED). Two approaches are presented: First, volumetric, porous structures with a defined shape are manufactured with L-PBF. Second, coatings are fabricated by L-DED with alternating process parameters, leading to local deviations of the magnetic permeability. This non-deterministic coding approach generates a distinctive material structure that triggers high signal amplitudes in the eddy current measurement. Counterfeiting becomes impossible due to the irreproducible melt pool dynamics. Statistical hypothesis testing proves that the system is able to prevent false acceptance or rejection of a code with a certainty of 500 million to one. A low-cost setup for a novel locking system demonstrates that a code can be sensed reliably within one second.

1. Introduction

Additive manufacturing (AM) is characterized by a layer-wise generation of a part. Raw material such as powder or wire is processed to build a coherent volumetric structure, determining the material properties during buildup. Most applications aim for a dense structure with isotropic mechanical properties. However, process-inherent deviations and imperfections can also be turned into valuable features for special purposes: Since AM enables a local manipulation of the process, there are various possibilities to design the material composition and microstructure for a specific objective as shown by Loh et al. [1], which is often referred to as tailored properties. Challenges arise from material science when multiple materials are combined as outlined by Tey et al. [2] and Bandyopadhyay and Heer [3], as well as from production engineering, since the toolpath and process parameters need to be adapted locally as shown by Steuben et al. [4]. Mitchell et al. [5] forges the bridge to 4D printing of “smart” materials, which means that they respond in a predefined way to an external stimulus.

Local process manipulation can also be used as a protection against counterfeiting of the part itself as proposed by Jahnke et al. [6] or for coding as integrated function, which improves the security of the manufacturing process as demanded by Yampolskiy et al. [7] and enables novel products for the security industry such as non-replicable keys. For these applications, the layer-by-layer fabrication is ideal as it enables internal, three-dimensional features that are not visible from the outside. As discussed by Kurfess and Cass [8], counterfeiting is a serious threat concerning confidence in engineering, since nearly any geometry can be produced by AM with stolen data or reverse engineering of an original product, but mechanical and functional properties of the replicated part may not be identical to the original ones and pose a safety risk. Thus, safety-critical industries such as automotive and aerospace demand for forgery-proof watermarks embedded in their AM parts.

A “code” carries secret information that can be read by a suitable device. For cryptography, code creation needs to be a controlled, deterministic process in order to be able to reproduce and decrypt a code. Some researchers use AM to generate deterministic codes: Chen et al. [9] embed a QR code as cavity in different polymers and metals. Wei

* Corresponding author.
E-mail address: eisenbarth@inspire.ethz.ch (D. Eisenbarth).

https://doi.org/10.1016/j.addma.2020.101298
Received 20 January 2020; Received in revised form 11 March 2020; Accepted 27 April 2020
Available online 24 May 2020

et al. [10] improve this approach by using two different materials to generate an internal QR code by powder bed AM. They test different sensing techniques such as infrared thermography, but only digital X-ray is successful in identifying these features reliably. A code can also be random and non-deterministic for the purpose of authentication. Well-known applications of random codes that are measured and matched to a stored reference are fingerprint or iris recognition as well as DNA profiling. For the artificial generation of a random code, the goal is to make an intentional reproduction of the pattern impossible, even if all manufacturing parameters are known. For instance, Ivanova et al. [11] embed nanoparticles of photopolymers into a part made by the polymer AM process of material jetting to create random patterns that can be visualized by a fluorescent microscope. Misfeldt et al. [12] patented an internal watermark formed by AM that is characterized by a different material density than the surface. Hocker [13] patented a sensing system that gathers any kind of information about the material characteristics and compares it to a reference value in order to check the authenticity of a raw material for an AM process.

When talking about unique coding, it is important to consider both the object to be measured and the measurement method with its resolution and accuracy. If a measurement technique is able to trace the material properties down to molecules, atoms, or even quantum states, then every object shows a unique, inherent coding, just because of the nearly endless number of physical states in matter and energy. With a higher measurement accuracy, finer differences of one property can be distinguished. Scanning electron microscopy or computed tomography scanning for instance come close to such ideal measurements, but are far too complex and costly for code reading on a daily basis. Unique coding for continuous usage requires two constituents: The creation of a code with enough distinguishing marks to be assumed to be unique, and a reading device that is able to detect the code unambiguously. This requires a mutual development of the manufacturing process and measurement technology as shown in here.

A unique code requires a large number of possible combinations, which are determined by the spatial and signal resolution of the reading device and the size of the scanned area or volume, hereafter called coding domain. One characteristic element of an arbitrary code is called artifact. In order to be detectable, the artifact size D_a needs to be equal or bigger than the resolution D_r of the reading device. For a unique code, enough artifacts need to be placed in the domain, thus D_a needs to be equal or smaller than the maximum size D_q that is required to reach a certain artifact quantity within the domain:

$$D_r \leq D_a \leq D_q \tag{1}$$

Here, the additive processes of laser powder bed fusion (L-PBF) and laser directed energy deposition (L-DED) are used to generate deterministic and non-deterministic codes in metallic parts by controlled and random process variation. These codes can be identified by an eddy current reading device, which allows robust and repeatable measurements. The eddy current hardware consists only of small coils and electronics, thus it can be designed for small, low energy applications and has the potential for low-cost mass production. Since the code is made up of local deviations inside the solid material and does not contain any electronics, it is immune to surface scanning methods and remote readings, which is for instance a vulnerability of RFID chips.

2. Materials and methods

2.1. Coding approach using L-PBF

L-PBF is an additive process that fuses a metallic powder bed selectively with a laser. By lowering the platform and recoating the powder bed, parts are fabricated layer by layer as illustrated in Fig. 1.

Rectangular parts from stainless steel type 1.4404 (316L) with a particle size distribution of $d_{10} = 11\,\mu m$, $d_{50} = 20\,\mu m$, and $d_{90} = 37\,\mu m$, delivered by Carpenter Ltd., are processed with L-PBF.

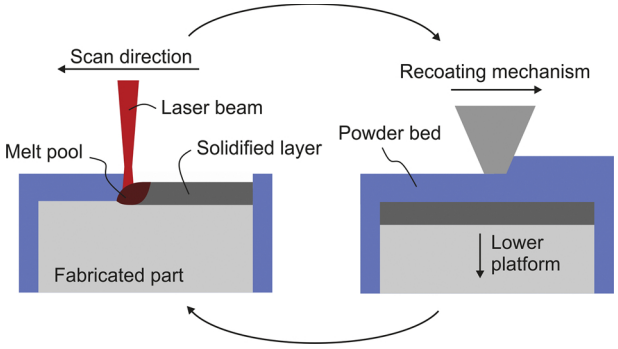

Fig. 1. L-PBF process: Powder bed fusion of one layer (left), lowering the platform and recoating (right) before the next layer is processed.

The first level of code creation is deterministic: Specific shapes with deviating material properties are defined in the 3D model of the part, which could form for instance a QR code. On the second level, the process parameters are manipulated in such way that intentional defects like pores occur randomly. Eddy current testing can detect these artifacts in electrically conductive materials, since inhomogeneities influence the electrical conductivity and magnetic permeability. Fig. 2 shows an exemplary 3D model that comprises coding domains of different size, shape, and material density, which could be determined by a random generator.

Melt pool dynamics have a stochastic character and can either cause a consistent or irregular manufacturing process. Yadroitsev et al. [14] show that certain parameter combinations with L-PBF lead to an irregular, non-predictable track shape and thus to randomly distributed defects. Stoffregen et al. [15] use the volume energy density E to influence the overall porosity of a part. For the L-PBF process, E is defined as

$$E = \frac{P}{vht} \tag{2}$$

It is calculated based on the four main process parameters, which are the laser power P, scan speed v, hatch distance h, and layer thickness t. If these process parameters are chosen in such a way that the volume energy density is low enough, a substantial and detectable amount of pores is created. These non-deterministic material characteristics of the solidified part shall be detected by the eddy current system. However, the volume energy density needs to be high enough to produce parts with a basic structural integrity. Fig. 3 plots the resulting relative density d_{rel} of parts produced by L-PBF as a function of the volume energy density E and for two different hatch distances h. The laser powder and layer thickness are kept constant with $P = 180\,W$ and $t = 30\,\mu m$. The scan speed v varies between 450 and 1150 mm/s.

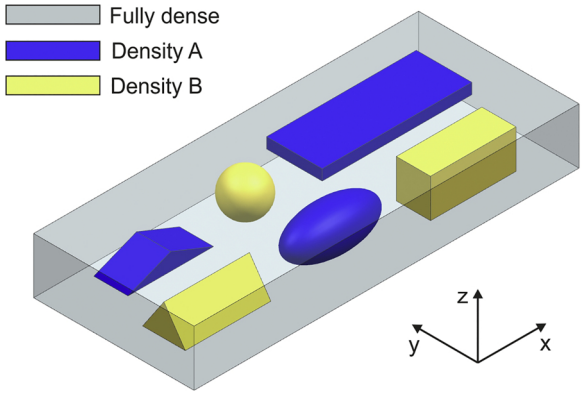

Fig. 2. Coding domains with different size, shape, and density in a rectangular part.

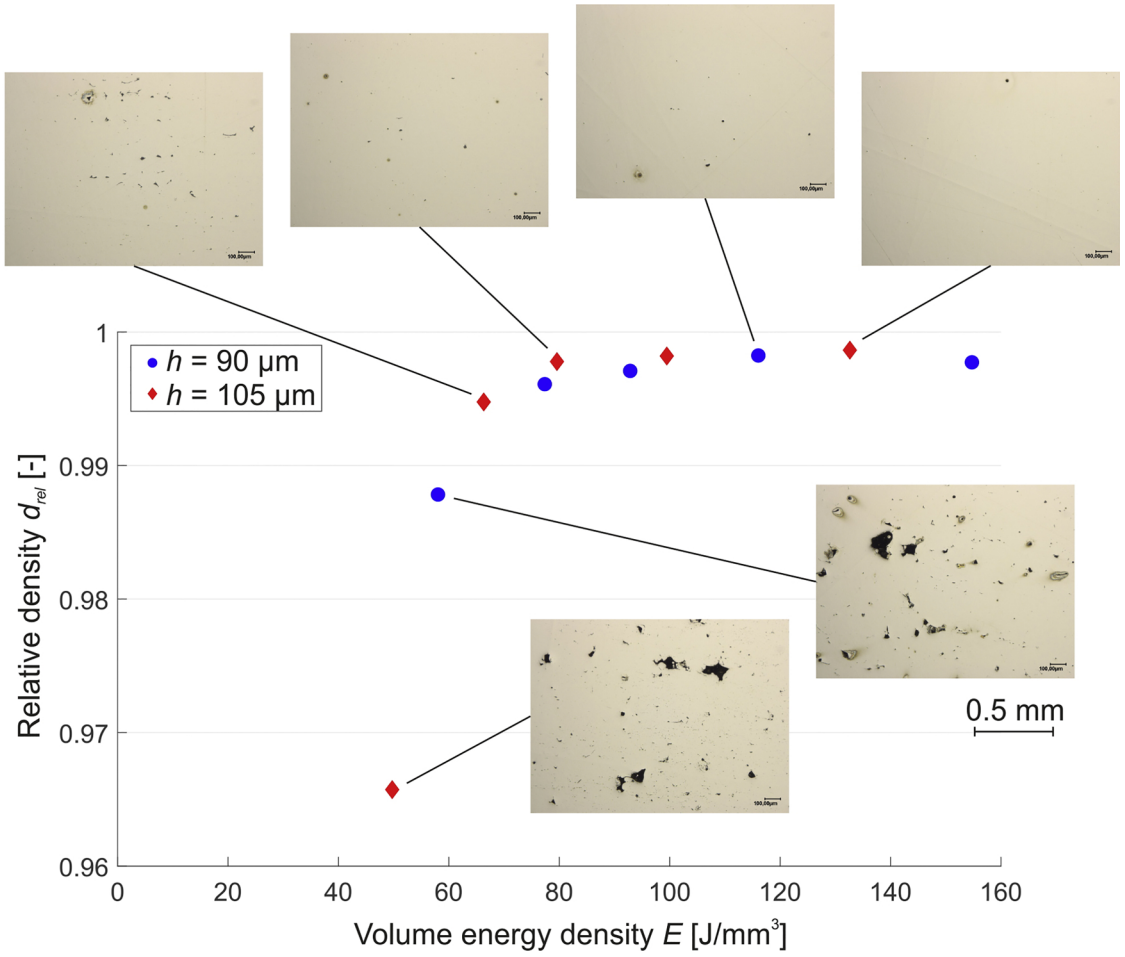

Fig. 3. Relative density d_{rel} as a function of the volume energy density E of L-PBF parts. Related cross sections show the level of porosity.

The relative density d_{rel} is defined as the measured density divided by the reference density of the corresponding bulk material. The cross sections show the typical material structure for different relative densities of steel type 1.2709 (MS1) processed by L-PBF. In this case, the density is only measured optically, that means based on single cross sections of the part. In comparison to density measurements according to Archimedes' principle, the optical method lacks global information for the entire part as stated by Spierings et al. [16]. In Fig. 3, it is clearly visible that the relative density decreases significantly for this type of steel as soon as the volume energy density drops below 70 J/mm^3.

Mechanical properties of the porous structure inside the coding domains are certainly inferior compared to a fully dense material and will show a high fluctuation due to the inhomogeneous structure. For the calculation of the part strength, it is reasonable to treat the coding domains as empty cavities. Furthermore, the codes need to be positioned in an accessible region of the part near the surface in order to be readable. Suitable applications for porous coding domains are unloaded edge regions or purely functional parts such as keys, thus it is not intended that they bear any loads.

2.2. Coding approach using L-DED

For the L-DED process, powder is blown directly into a melt pool created by a laser as illustrated in Fig. 4. By overlapping these spherical tracks, layers and volumetric structures are created. The process needs to start on a base material and can apply different powder materials for each layer or for a final coating.

L-DED can be applied to any solid body made from a weldable base material. In contrast to the L-PBF approach, the magnetic

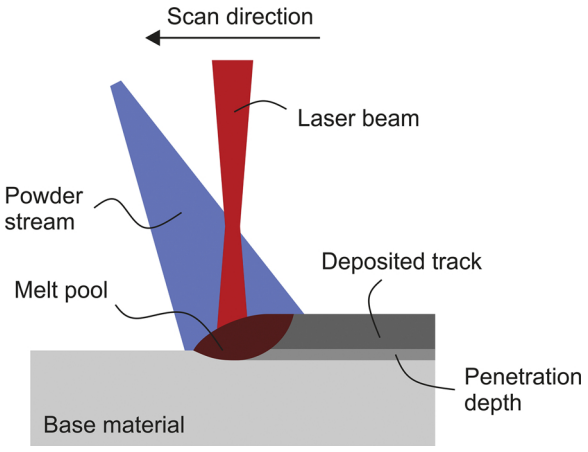

Fig. 4. L-DED process: Powder is blown into a melt pool created by a laser.

characteristics of two materials can be used for code creation, since the implementation of a multi-material process is straightforward with L-DED. Eddy current testing is very sensitive to the magnetic permeability μ, which is the derivation of the magnetic induction $\underline{B}$ in a material with respect to an external magnetic field $\underline{H}$ and can be written for incremental steps as:

$$\Delta \underline{B} = \mu \Delta \underline{H} \tag{3}$$

The relative permeability is $\mu_r = \mu/\mu_0$ with μ_0 as the permeability of vacuum, which is approximately $4\pi \times 10^{-7} N A^{-2}$. Eddy current testing

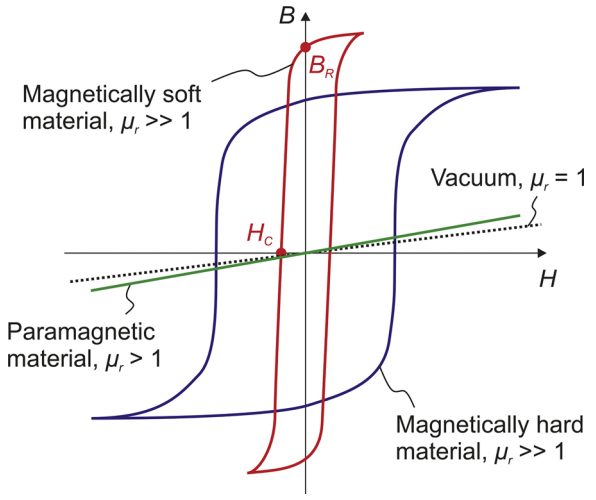

Fig. 5. Exemplary hysteresis curves for paramagnetic, magnetically soft, and magnetically hard materials.

as applied here does not measure the actual state of magnetization, which is the principle of hard drives and recording tapes, but the magnetic permeability of the material. The permeability as described by the hysteresis curve is an inherent material characteristic and is mostly constant for a specific magnetic field and constant environmental conditions. In contrast to magnetic storage, it is therefore not possible to overwrite a code inscribed in the magnetic permeability after the material has solidified in the manufacturing process.

For code creation, magnetically soft steel is locally mixed with paramagnetic steel in the melt pool, resulting in a microstructure with specific magnetic properties as the material solidifies. Paramagnetic steel has a relative permeability slightly above one, causing a flat hysteresis curve that transitions into a straight line with low permeability and no remanence, which means that a given magnetic field $\underline{H}$ does barely increase the magnetic induction $\underline{B}$ in the material. In contrast, magnetically soft steel shows a steep hysteresis curve with high permeability μ_r and remanence B_R but low coercivity H_C, thus it is easy to magnetize, but does not keep its state of magnetization as rigidly as magnetically hard steel. Exemplary hysteresis curves for paramagnetic, magnetically soft and hard materials are depicted in Fig. 5. A deep analysis of magnetic properties is given by Yang et al. [17], who process magnetically soft steel by L-DED and show that both the alloy composition and the process parameters influence the magnetic properties. In particular, directional grains promote magnetic anisotropy.

The base material for the experiments as shown here is a magnetically soft low carbon steel type 1.0332 (DD11). Typical ferritic steel shows a relative permeability μ_r between 500 and 2000 according to Fofanov and Riedner [18]. Austenitic powder type 1.4404 (316L) from Carpenter Ltd. as slightly paramagnetic material is deposited atop, for which a relative permeability $\mu_r = 1.25$ is reported. The particle size ranges between 45 and 106 µm. The high difference in permeability shall result in a high contrast during eddy current testing. Regarding the process parameters of L-DED, the laser power P and scan speed v determine the penetration and dilution of the base material. By altering the process parameters P and v locally, the depth of the melt pool, the magnitude of dilution, and the heat affected zone in the base material are varied within specific boundaries. This controlled, deterministic process variation is transformed into a stochastic, non-deterministic process by using a random generator for toolpath and process parameter creation. In addition, the overlapping tracks lead to interdependencies of the parameters at different locations. It is aspired that the permeability scatters significantly and randomly across the coding domain.

Table 1 sums up the approaches of code creation with L-PBF and L-DED. Formation of the microstructure is a non-deterministic process based on probabilities due to the irregular melt pool dynamics in both fabrication methods. Formation of the macrostructure is a controlled mechanism and therefore deterministic. However, by using a random generator for instance for the CAD model generation and parameter variation, an exact reproduction of the code becomes practically impossible.

Table 1
Approaches of code creation with L-PBF and L-DED.

Scale	Micro	Macro
Code creation	Random	Controlled
L-PBF	Size and distribution of pores	CAD model
L-DED	Dilution and penetration depth	Parameter variation

2.3. Code reading by eddy current

Eddy current examination is a technology standardized by ISO 15548-1 [19] to detect defects inside electrically conductive materials without destroying the part. An excitation coil is positioned above the test specimen and an alternating current with a specific amplitude and frequency is applied as shown by Fig. 6. The changing primary magnetic field produces eddy currents in the conductive material. Changes in the material structure and defects in the part show a different electrical conductivity and magnetic permeability, leading to an amplitude change and phase shift of the eddy currents, which create a deviating secondary field opposed to the primary one. The secondary field can be detected by measuring the impedance change in the excitation coil or by using a second reception coil.

The main input parameter for eddy current testing is the excitation frequency. The penetration depth and sensitivity describe the performance of the measurement technique. The standard penetration depth δ is defined as the depth at which the eddy current intensity drops to $1/e \approx 37\%$ of the surface intensity. It depends on the eddy current frequency f, the permeability μ and electrical conductivity κ of the material and is approximated as:

$$\delta = \frac{1}{\sqrt{\pi f \mu \kappa}} \tag{4}$$

The depth of penetration is therefore low for materials with high permeability and electrical conductivity such as ferritic steel, which can be explained by a strong secondary magnetic field that forms near the surface, counteracting the primary field as further explained by Prasad and Nair [20]. Szczyglowski [21] states that a high frequency decreases the depth of penetration and leads to energy losses during re-

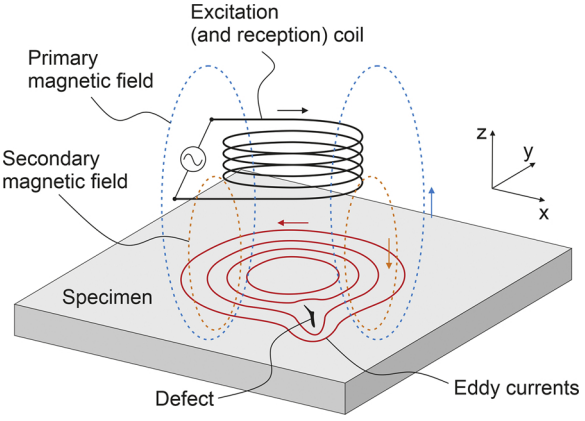

Fig. 6. Schematic illustration of eddy current testing with a distorted eddy current flow due to a defect in the test specimen.

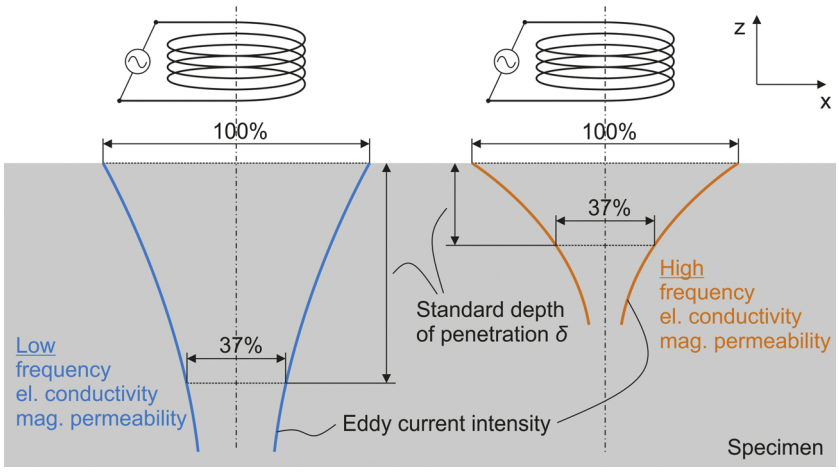

Fig. 7. Eddy current intensity inside the specimen with high (left) and low (right) standard depth of penetration.

magnetization. Sensitivity refers to the change in signal when the material properties vary locally as caused by a defect. A higher frequency increases in general the sensitivity as shown by Zhou et al. [22]. The highest sensitivity is obtained at the surface, and the exponential decrease of the eddy current intensity inside the material reduces the sensitivity accordingly. Fig. 7 illustrates the influence of the parameters for defect detection: With a low frequency, deep defects can be sensed but with low sensitivity, which means that they need to be large and distinctive compared to the surrounding. A high frequency can detect small defects with high sensitivity, but only near the surface. The choice of the excitation frequency is therefore a trade-off between measurement depth and resolution.

2.4. Measurement setup

15 specimens are fabricated by L-PBF and L-DED, respectively and measured by eddy current. The nominal size of all specimens is 27.5 × 7.5 mm, with a thickness of 3.6 mm. Two eddy current measurement setups are used for validation: For the academic setup, an eddy current sensor is mounted on a linear stage and measures a grid in x and y, enabling a high-resolution 2D image of the coding domains. The industrial 1D setup uses one eddy current sensor coupled with a linear position sensor and scans one line in the middle of the specimen. The 2D setup is intended for analysis and validation of the developed L-PBF and L-DED processing approaches, whereas the 1D setup is designed for easy and fast authentication and serves as a prototype for a future implementation of the technology. Parameters considering measurement of one specimen are listed in Table 2.

3. Results and discussion

3.1. 2D measurement of L-PBF codes

Each L-PBF specimen possesses two rectangular coding domains with a size of 9.2 × 5.7 mm and a thickness of 2.2 mm, processed with

Table 2
Measurement parameters for 2D and 1D eddy current testing.

Setup	Academic (2D)		Industrial (1D)
Specimens	L-PBF	L-DED	L-DED
Eddy current frequency [kHz]	521	200	1097
x resolution [mm]	0.12	0.12	0.025
y resolution [mm]	0.5	0.1	N/A
Measured points (one spec.)	3400	17,000	800
Acquisition time (one spec.) [s]	11	53	1

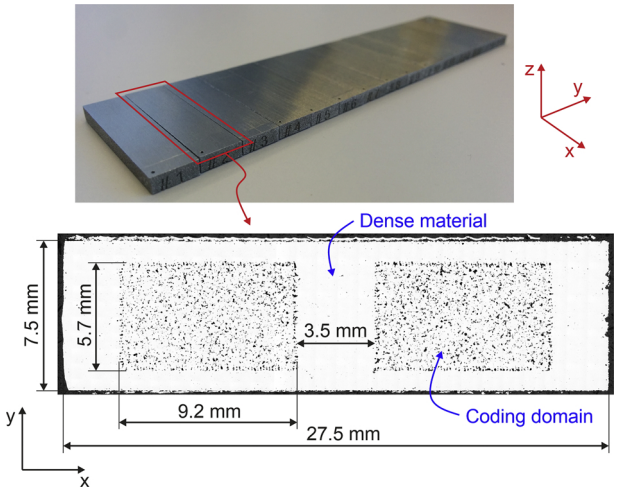

Fig. 8. Ground L-PBF specimens (top), cross section in the x-y-plane with two porous coding domains (bottom) with a relative density of 73%.

different scan speeds and thus different volume energy densities. The coding domains are centered in the z-direction, thus the dense top layer is 0.7 mm thick. Fig. 8 depicts the L-PBF specimens after grinding of the surface and a cross section of one specimen in the x-y-plane with the lowest volume energy density of $E = 21.4\,\mathrm{J/mm^3}$, leading to a relative density of $d_{rel} = 73\%$.

Fig. 9 depicts the data of the 2D measurement of five L-PBF specimens, with the output voltage U_{out} of the eddy current device in pseudo-colors. A cubic interpolation is applied to create a continuous plot. The specimens are labeled with numbers, and the nominal specimen size is indicated in blue. The coding domains of specimen 1 are built with the lowest scan speed of 1800 mm/s and therefore highest volume energy density. The domains of specimens 2 and 3 are built with 2300 mm/s, and the domains of specimens 4 and 5 with 2800 mm/s, thus with the lowest volume energy density. The default scan speed to achieve a material density $d_{rel} > 99.5\%$ while keeping the other three parameters constant according to Eq. (2) is 1000 mm/s. The coding domains are clearly distinguishable from the dense areas for specimens 2 to 5. The white background area in Fig. 9 depicts free space with a measurement signal $U_{out} \leq -0.15\,\mathrm{V}$. The red areas with $U_{out} \geq 0\,\mathrm{V}$ show the specimens. Readings in between these values are due to edge effects of the measurement. The specimen width in y-direction appears to be smaller compared to the nominal geometry, since the eddy current device travels along the x-axis and creates a slightly direction-dependent signal.

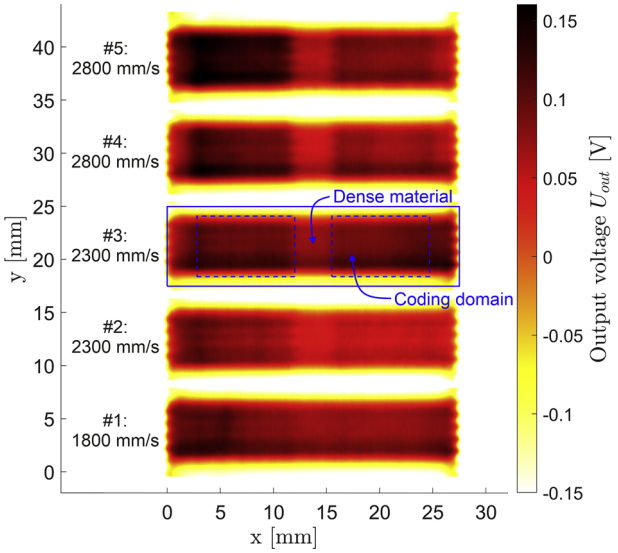

Fig. 9. 2D eddy current measurement of five specimens made by L-PBF with different scan speeds. The output voltage is shown in pseudo-colors.

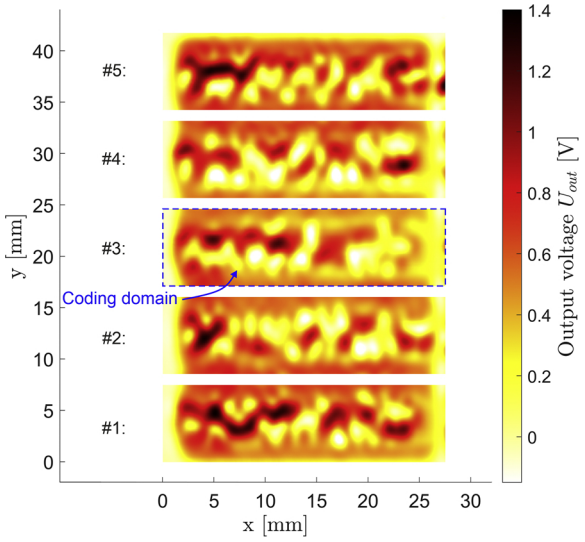

Fig. 11. 2D eddy current measurement of five specimens made by L-DED. The output voltage is shown in pseudo-colors.

The eddy current system is not able to detect single pores as visible in the cross section in Fig. 8, since the depth of the coding domain requires a low eddy current frequency, leading to a low resolution and sensitivity. However, the measurement is able to indicate the average density of the coding domains: In the porous areas of specimens 4 and 5 made with the highest scan speed, the highest output voltage of $U_{out} = 0.15$ V is measured, compared to $U_{out} = 0.06$ V in the dense area between the two coding domains. For specimen 1, the similarity of the dense and porous area prevents a detection with the present eddy current setup: The number and size of the pores are too low to modify the average material density sufficiently for the given sensitivity of the measurement. It is assumed that unmelted powder remaining in the porous structure does not impair the sensor reading, since the number and size of the defects determines the magnetic permeability and the eddy current signal. Thus, the difference between a gas-filled and a partly powder-filled pore is negligible compared to the influence of the pore geometry.

3.2. 2D measurement of L-DED codes

The coding domain made with L-DED covers the entire specimen. Deposition takes place on a large plate that is ground and cut subsequently to obtain the specimens as depicted in Fig. 10. An exemplary etched cross section in the *x*-*z*-plane shows the ferritic base material and the deposited austenitic steel. Pretests reveal that a laser power P between 500 and 1150 W combined with a scan speed v between 700 and 900 mm/min leads to promising results regarding the artifact size of the code. A random generator changes the laser power and scan speed within these limits and creates the NC code for processing. As visible from the cross section, the parameter variation results in the intended non-deterministic, non-uniform melt pool depth, lying between 0.5 and 1 mm below the surface.

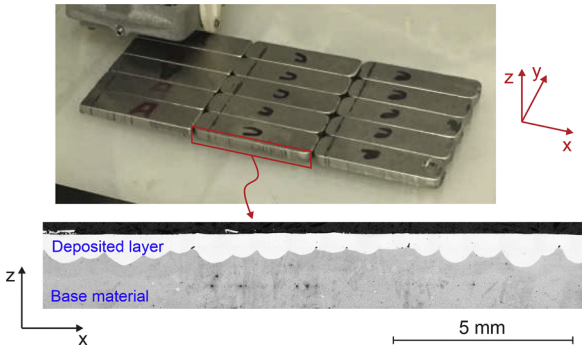

Fig. 10. Ground and cut L-DED specimens (top), etched cross section in *x*-*z*-plane (bottom), showing the low carbon steel as base material and the deposited austenitic steel.

2D eddy current measurements of five specimens are shown in Fig. 11. The specimens 1 to 5 are fabricated under identical conditions, except for the random variation of the process parameters P and v within the limits mentioned above. As crucial for a unique code, the eddy current signal does not show any recurring patterns or areas of constant value. The specimens reveal a multitude of distinguishing marks resulting from the varying magnetic permeability with a pitch between 1 and 3 mm. The acquired signal varies by 1.4 V, which is 9 times higher than the signal variation of the L-PBF specimens. One reason is that the L-DED approach varies directly the magnetic permeability on a large scale due to the two materials and the alternating process parameters, whereas the L-PBF approach generates small pores that have an even smaller influence on the permeability of the conductive material. Due to the limitations of the eddy current technology as described above, the L-PBF approach can only generate deterministic codes that are defined in the 3D model, since the non-deterministic pore distribution is below the resolution of the eddy current measurement. The L-DED approach generates non-deterministic, distinguishable marks and is subsequently analyzed regarding its robustness and reliability.

3.3. Statistical hypothesis testing of L-DED codes

The development of a non-deterministic coding system leads to three conflicting goals: First, the number of possible combinations to reach a level of uniqueness, second, the reliability of authentication, and third, the measurement effort in terms of hardware and software complexity of the reading device, influencing the performance and costs. The number of combinations and the reliability are analyzed by statistical hypothesis testing with the measurement results from the 15 L-DED specimens.

Authentication is done by a comparison of target and actual values: An industrial reading device would only measure a certain number of positions in the coding domain for fast processing. If all of these measurements comply with the stored target value, the reading device accepts the code. If one or more measurements do not match, the code is

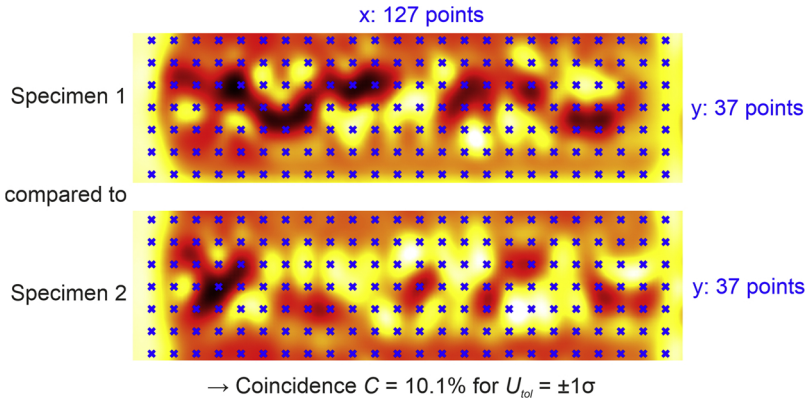

Fig. 12. Exemplary comparison of L-DED specimen 1 to 2, regarding the coincidence of a grid of 127 × 37 data points.

rejected. The null hypothesis is defined as "device reads an authentic code". A reliable system must be designed to prevent type 1 and type 2 errors with a high probability. A type 1 error leading to a false positive result is defined as "device reads an authentic code but rejects it". A type 2 error leading to a false negative result is defined as "device reads an unauthentic code but accepts it". Type 1 errors can be prevented by a high measurement tolerance. It is assumed that random measurement deviations follow a normal distribution with a specific standard deviation σ. In quality assurance, the three- and six-sigma rules are common to define a tolerance range for normally distributed events: A limit of $\pm 1\sigma$ from the mean gives a certainty of 68.3% that a value lies within the acceptable range. A limit of $\pm 3\sigma$ gives a certainty of 99.7%. Applying a limit of $\pm 6\sigma$, the probability for an outliner is less than one to 500 million. However, a high sigma range increases the probability of type 2 errors. The standard deviation is assumed to be $\sigma = 0.0228$ V here, which is the measurement uncertainty of the eddy current device in free space. All L-DED codes are compared to each other on the basis of a data grid of 127 × 37 points, as shown exemplarily in Fig. 12 for specimens 1 and 2.

For a tolerance range $U_{tol} = \pm 0.0228\,\text{V} = \pm 1\sigma$, a fraction of 10.1% of the 4699 measurement points of specimen 1 lie in the tolerance range of specimen 2. In general, this fraction called coincidence C is defined as the total number of matches K divided by all measurement points N of each coding area:

$$C = \frac{K}{N} \tag{5}$$

Comparing all 15 L-DED codes to each other gives an adequate statistical basis of 105 samples. The resulting maximum coincidence C_{max} is 12.3% for a tolerance range of $\pm 1\sigma$. The tolerance range influences the magnitude of coincidence. Fig. 13 plots the maximum coincidence as the worst-case combination of the 15 codes versus the applied tolerance range. C_{max} drops to zero if the tolerance band is zero, and reaches one as soon as the tolerance range covers the entire signal

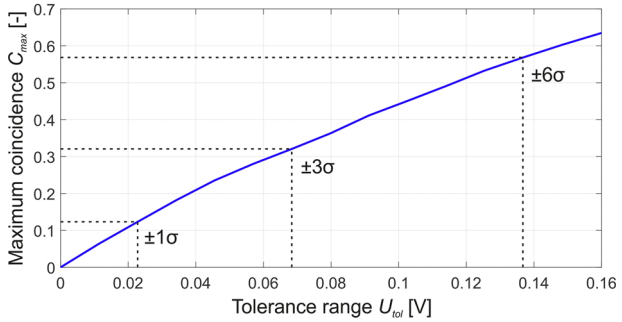

Fig. 13. Maximum coincidence of two different codes as a function of the tolerance range. C_{max} at one, three, and six sigma is indicated by dashed lines.

amplitude. A three-sigma range results in a coincidence C_{max} of 32%. A six-sigma range, which is favorable to prevent type 1 errors, leads to $C_{max} = 57\%$.

However, a high coincidence does not necessarily lead to a high probability of type 2 errors, since all chosen measurement points need to match for code acceptance. The question is, how many measurement points are actually necessary to prevent both type 1 and type 2 errors. Fewer measurement points reduce the complexity of the hardware and enable a faster data processing. The probability of type 2 errors can be calculated by the hypergeometric distribution. It describes the probability mass function P to obtain exactly $X = k$ matches in a random sample size n:

$$P(X = k) = \frac{\binom{K}{k}\binom{N-K}{n-k}}{\binom{N}{n}} \tag{6}$$

All variables are natural numbers. The notation of Eq. (6) uses the binomial coefficient:

$$\binom{K}{k} = \frac{K!}{k!(K-k)!} \tag{7}$$

Here, n is the number of actual measurement points and k is the related subset of measurements lying in the tolerance range and are therefore declared as coincident by the reading device. As defined above, authentication requires a 100% match with k equal to n. $P(X = k = n)$ describes the probability of a type 2 error, which means that the reading device measures by accident only points that coincide, although the total coincidence of the two compared codes is less than one:

$$P(X = k = n) = \frac{\binom{K}{n}\binom{n-K}{0}}{\binom{N}{n}} = \frac{\binom{K}{n}}{\binom{N}{n}}, \quad \forall \; n \in [1, K] \tag{8}$$

Eq. (8) can be approximated for low coincidence C and small sample size n as a function to the power of n:

$$P(X = n) \approx \left(\frac{K}{N}\right)^n \tag{9}$$

This probability $P(X = n)$ is plotted as a function of the sample size n for three different tolerance ranges in Fig. 14, using a logarithmic scale for the y-axis.

With a sample size of $n = 1$, the probability for a type 2 error is equal to the coincidence C of Fig. 13. With an increasing sample size, the probability for an exact match drops significantly. When applying a tolerance range of $\pm 6\sigma$ to prevent type 1 errors, only 36 measurement points are required for this setup to prevent also type 2 errors with a probability of greater than 500 million to one. A high coincidence is therefore not detrimental per se, but increases the required number of

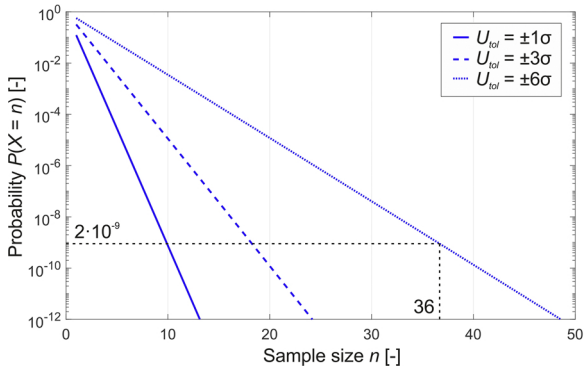

Fig. 14. Hypergeometric distribution with logarithmic *y*-axis: Probability of two different codes matching exactly, depending on the sample size and the applied tolerance range.

measurement points to achieve the same probability to prevent type 2 errors. Thus, an industrial reading device could use either 36 or more single eddy current coils for a static measurement, or fewer coils that are moved to different positions to capture 36 or more points. Erroneous acceptance or rejection of the code can then be both excluded with a certainty of 500 million to one.

3.4. Industrial setup for 1D measurement

A low-cost measurement device for L-DED codes has been developed as a demonstrator for a novel, high-security locking system and is depicted in Fig. 15. When a specimen is plugged into the slot, an eddy current sensor measures one line in the center and a position sensor correlates the output signal with the longitudinal coordinates. A Raspberry Pi microcomputer is used to compare the position-dependent signal with stored references for authentication. The sensor measures up to 800 points on a length of 20 mm, which takes approximately one second.

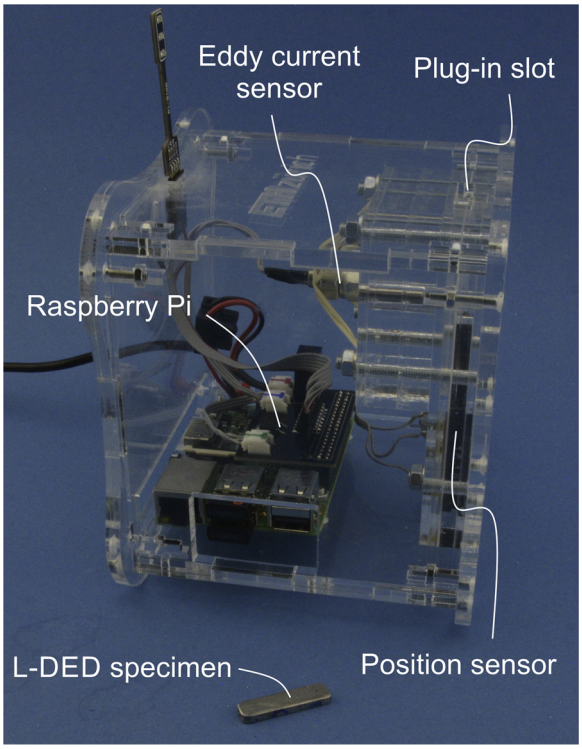

Fig. 15. Demonstrator for a high-security locking system. For the eddy current measurement, the specimen representing the key needs to be plugged into a slot representing the lock.

Fig. 16 shows the 1D output signal from eight different L-DED specimens, normalized between their minimum and maximum amplitude. Every specimen shows a distinctive pattern, although only one line is measured instead of the entire surface. The frequency of the 1D sensor is 1097 kHz compared to 200 kHz of the 1D sensor as used for the measurements in Fig. 11. Thus, the 1D sensor measures with a higher spatial resolution but slightly closer to the surface compared to the 2D sensor. The moving sensor shows larger deviations than a static measurement, leading to a maximum coincidence of C_{max} = 77% for a six-sigma approach. According to Eqs. (5)–(9), 74 measurement points are required here to prevent type 2 errors with a probability of greater than 500 million to one. Evaluating 800 measurement points as done here enables a very high reliability. All 15 L-DED specimens could be authenticated unambiguously without any type 1 or type 2 errors in multiple measurements. Common environmental influences such as temperature changes, magnetic fields, and finger sweat were tested but do not show a significant impact on the measurement signal beyond the standard deviation.

4. Conclusion

The additive processes L-PBF and L-DED are used to manufacture parts with an intentionally inhomogeneous and imperfect structure to create codes for authentication and anti-counterfeiting applications. The main results are summarized as follows:

- The artifacts that form the code need to be larger than the resolution of the chosen reading device, but small enough to reach a certain quantity of distinguishing marks for a unique code.
- With L-PBF, porous structures are fabricated with a reduced volume energy density. Small pores cannot be detected individually, but the eddy current device is able to indicate the average porosity of an area, which can be used to detect deterministic codes.
- With L-DED, a varying melt pool depth and dilution of two materials with different magnetic permeability are generated by alternating process parameters. Since eddy current testing is sensitive to magnetic properties, the coding area triggers a distinctive, non-deterministic signal.
- The probability of erroneous acceptance or rejection of a code is calculated with statistical hypothesis testing. It is demonstrated that the L-DED approach is reliable with a certainty of 500 million to one, if a certain number of measurement points is used depending on the measurement uncertainty of the eddy current device.
- A demonstrator for a novel locking system with low-cost components shows that the 15 specimens fabricated by L-DED could be authenticated unambiguously within one second.

In future, code generation could be easily implemented in existing additive manufacturing processes in order to tag every part with a code just below the surface. For the L-PBF process and its resulting small pores, advanced measurement equipment is needed for code detection. The L-DED process reveals that both the fabrication and measurement approach are mature for an easy and fast authentication of codes, for instance for new security products and continuous part tracking throughout the product lifecycle.

Funding

This work was supported by the Swiss Innovation Agency*Innosuisse* [grant number 19246].

Authors' contributions

Daniel Eisenbarth: Methodology, Investigation, Validation, Visualization, Writing – Original Draft

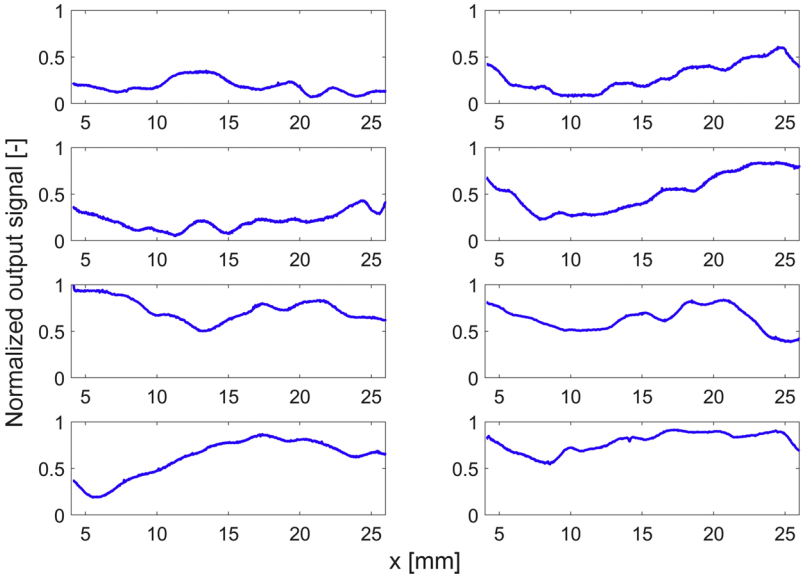

Fig. 16. Normalized output signals from the industrial setup as a function of the longitudinal *x*-position for eight L-DED specimens.

Philipp Stoll: Methodology, Investigation, Validation, Writing – Review & Editing

Christoph Klahn: Conceptualization, Methodology, Investigation, Writing – Review & Editing

Timon B. Heinis: Software, Investigation, Validation, Writing – Review & Editing

Mirko Meboldt: Conceptualization, Resources, Supervision, Writing – Review & Editing

Konrad Wegener: Conceptualization, Resources, Supervision, Writing – Review & Editing

Conflicts of interest

The authors declare no conflicts of interest.

Acknowledgments

The authors would like to thank Samuel Blösch for his support and acknowledge the contribution of the funding agency *Innosuisse* and of the company *dormakaba Holding AG*.

References

[1] G.H. Loh, E. Pei, D. Harrison, M.D. Monzon, An overview of functionally graded additive manufacturing, Addit. Manuf. 23 (2018) 34–44, https://doi.org/10.1016/j.addma.2018.06.023.

[2] C.F. Tey, X. Tan, S.L. Sing, W.Y. Yeong, Additive manufacturing of multiple materials by selective laser melting: Ti-alloy to stainless steel via a Cu-alloy interlayer, Addit. Manuf. 31 (2018) 100970, https://doi.org/10.1016/j.addma.2019.100970.

[3] A. Bandyopadhyay, B. Heer, Additive manufacturing of multi-material structures, Mater. Sci. Eng.: R: Rep. 129 (2018) 1–16, https://doi.org/10.1016/j.mser.2018.04.001.

[4] J.C. Steuben, A.P. Iliopoulos, J.G. Michopoulos, Implicit slicing for functionally tailored additive manufacturing, Comput.-Aided Des. 77 (2016) 107–119, https://doi.org/10.1016/j.cad.2016.04.003.

[5] A. Mitchell, U. Lafont, M. Holynska, C. Semprimoschnig, Additive manufacturing – a review of 4d printing and future applications, Addit. Manuf. 24 (2018) 606–626, https://doi.org/10.1016/j.addma.2018.10.038.

[6] U. Jahnke, C. Lindemann, M. Moi, R. Koch, Potentials of additive manufacturing to prevent product piracy, Proceedings of the 24th International Solid Freeform Fabrication Symposium (2013).

[7] M. Yampolskiy, W.E. King, J. Gatlin, S. Belikovetsky, A. Brown, A. Skjellum, Y. Elovici, Security of additive manufacturing: attack taxonomy and survey, Addit. Manuf. 21 (2018) 431–457, https://doi.org/10.1016/j.addma.2018.03.015.

[8] T. Kurfess, W.J. Cass, Rethinking additive manufacturing and intellectual property protection, Res.-Technol. Manag. 57 (2014) 35–42, https://doi.org/10.5437/08956308X5705256.

[9] F. Chen, Y. Luo, N.G. Tsoutsos, M. Maniatakos, K. Shahin, N. Gupta, Embedding tracking codes in additive manufactured parts for product authentication, Adv. Eng. Mater. (2018) 1800495, https://doi.org/10.1002/adem.201800495.

[10] C. Wei, Z. Sun, Y. Huang, L. Li, Embedding anti-counterfeiting features in metallic components via multiple material additive manufacturing, Addit. Manuf. 24 (2018) 1–12, https://doi.org/10.1016/j.addma.2018.09.003.

[11] O. Ivanova, A. Elliott, T. Campbell, C.B. Williams, Unclonable security features for additive manufacturing, Addit. Manuf. 1–4 (2014) 24–31, https://doi.org/10.1016/j.addma.2014.07.001.

[12] Misfeldt E.D., Allott M.T., Pierz S.J., Component and watermark formed by additive manufacturing, Patent number US9374497B2, 2016.

[13] Hocker T., Identifying a characteristic of a material for additive manufacturing, Patent number US2018001565A1, 2018.

[14] I. Yadroitsev, A. Gusarov, I. Yadroitsava, I. Smurov, Single track formation in selective laser melting of metal powders, J. Mater. Process. Technol. 210 (2010) 1624–1631, https://doi.org/10.1016/j.jmatprotec.2010.05.010.

[15] H. Stoffregen, J. Fischer, C. Siedelhofer, E. Abele, Selective laser melting of porous structures, Proceedings of the 22nd International Solid Freeform Fabrication Symposium (2011) 680–695.

[16] A.B. Spierings, M. Schneider, R. Eggenberger, Comparison of density measurement techniques for additive manufactured metallic parts, Rapid Prototyp. J. 17 (2011) 380–386, https://doi.org/10.1108/13552541111156504.

[17] X. Yang, X. Cui, G. Jin, J. Liu, Y. Chen, Z. Liu, Soft magnetic property of (fe60-co35ni5)78 si6b12cu1mo3 alloys by laser additive manufacturing, J. Magn. Magn. Mater. 466 (2018) 75–80, https://doi.org/10.1016/j.jmmm.2018.06.085.

[18] D. Fofanov, S. Riedner, Magnetic properties of stainless steels: applications, opportunities and new developments, Proceedings of the 2011 World Stainless Steel Conference, Vol. 29 (2011) 1–13.

[19] ISO 15548-1, Non-Destructive Testing – Equipment for Eddy Current Examination – Part 1: Instrument Characteristics and Verification, (2013).

[20] J. Prasad, C.K. Nair, Non-Destructive Testing and Evaluation of Material, Tata McGraw-Hill Education, 2011 ISBN 9780070707030.

[21] J. Szczyglowski, Influence of eddy currents on magnetic hysteresis loops in soft magnetic materials, J. Magn. Magn. Mater. 223 (2001) 97–102, https://doi.org/10.1016/S0304-8853(00)00584-9.

[22] D. Zhou, X. Chang, Y. He, H. Wang, P. Cao, L. Yang, Influence of key factors on eddy current testing sensitivity and monotonicity on subsurface depth for ferromagnetic and non-ferromagnetic materials, Sens. Actuators A: Phys. 278 (2018) 98–110, https://doi.org/10.1016/j.sna.2018.05.018.